Muon Imaging for Cu-Fe Ore Shoot Identification: Results and Next Challenges

Tommaso Beni,[1,2] Diletta Borselli,[2,3,4] Lorenzo Bonechi,[2] Massimo Bongi,[2,4] Debora Brocchini,[5] Roberto Ciaranfi,[2] Luigi Cimmino,[6,7] Vitaliano Ciulli,[2,4] Raffaello D'Alessandro,[2,4] Andrea Dini,[8] Catalin Frosin,[2,4] Giovanni Gigli,[1] Sandro Gonzi,[2,4] Silvia Guideri,[5] Luca Lombardi,[1] Massimiliano Nocentini,[1] Giulio Saracino,[6,7] and Nicola Casagli[1]

[1]*Department of Earth Sciences, University of Florence, Via Giorgio La Pira 4, 50121 Florence, Italy*

[2]*National Institute for Nuclear Physics INFN, Division of Florence, Via Bruno Rossi 1, 50019 Sesto Fiorentino, Italy*

[3]*Department of Physics and Geology, University of Perugia, Via Alessandro Pascoli, 06123 Perugia, Italy*

[4]*Department of Physics and Astronomy, University of Florence, Via Giovanni Sansone 1, 50019 Sesto Fiorentino, Italy*

[5]*Parchi Val di Cornia S.p.A., Via Giovanni Lerario 90, 570254 Piombino, Italy*

[6]*Department of Physics "Ettore Pancini", University of Naples Federico II, Via Cinthia 21, 80126 Naples, Italy*

[7]*National Institute for Nuclear Physics INFN, Division of Naples, Via Cinthia, 80126 Naples, Italy*

[8]*Institute of Geosciences and Georesources CNR, 56127 Pisa, Italy*

Corresponding author: Tommaso Beni
Email: tommaso.beni@unifi.it

Abstract

Transmission-based muography (TM) is becoming an innovative and nondestructive imaging technique based on the measurement of the cosmic ray muon flux attenuation within matter, allowing the reconstruction of two- or three-dimensional transmission and density polar maps. This paper presents our most recent findings on TM measurements applied to ore shoot prospecting. All measurements and results were obtained during the MIMA-SITES project years of research. The case study was the Temperino mine in the San Silvestro Archaeological and Mining Park (Campiglia Marittima, Italy). Here, several magmatic and metasomatic geological units outcrop. Among them is a Cu-Fe-Zn-Pb(-Ag) sulfide skarn complex primarily composed of hedenbergite and ilvaite minerals.

Keywords: cosmic ray, muography, ore shoot, geophysics, mining prospection
DOI: 10.31526/JAIS.2024.468

1. INTRODUCTION

Geologists, mining experts, and rock engineers have always desired to "visualize" the internal structure of rock masses, analogous to how X-ray radiography techniques penetrate the human body, allowing the reconstruction of an image. Currently, there are only a few methods for imaging the inner parts of a rock mass. These include core drilling, which involves the direct extraction of rock cores, as well as conventional nondestructive geophysical methods such as seismic imaging, gravity measurements, ground-penetrating radar, electromagnetic techniques, and gravity-based approaches. Underground core drilling encounters significant logistical and spatial challenges because of its cost-prohibitive nature, thereby restricting the feasibility of conducting numerous investigations and perpetuating an inherent level of uncertainty. Conversely, noninvasive geophysical techniques encounter complexities when employed in underground mining and rock engineering settings owing to factors such as logistical expenses, limited resolution, and installation intricacies. Despite this, they can provide a larger but less specific insight into the geological structure of the surrounding rock formations. In this context, the muon imaging technique is developing as a cost-effective and trustworthy booster for both invasive and noninvasive consolidated survey techniques in the underground mining field [1, 2, 3, 4]. For this purpose, the MIMA detector prototype (Muon Imaging for Mining and Archaeology; a cubic detector of $0.4 \times 0.4\,\mathrm{m}^2$ active surface), implemented during the MIMA-SITES research project, was used [1, 4, 5]. The MIMA tracker is a small and rugged muon tracker developed by physicists of the National Institute for Nuclear Physics (INFN) and the Department of Physics and Astronomy of Florence [6, 7, 8]. The front-end electronics and DAQ of the MIMA detector were implemented based on the knowledge and expertise of the muon radiography of Vesuvius experiment MURAVES [9, 10].

The case study was the Temperino mine in the San Silvestro Archaeological and Mining Park (Figure 1) [1]. The geological succession of events that characterize this area, allowing the enrichment of the skarn body with Cu-Fe-Zn-Pb(-Ag) sulfide, can be summarized as follows [11, 12, 13]:

(1) emplacement of the Botro ai Marmi monzogranite pluton that created an extended contact-metamorphic aureole (marble host rocks) and triggered metasomatic processes that created several skarn bodies,

(2) the intrusion of mafic porphyry dikes in the Temperino mining area, associated with skarn bodies (never directly intruding the marble),

(3) the intrusion of the felsic porphyry (Coquand felsic dike and Ortaccio felsic dike) that crosses all the older contacts and lithologies, forming epidosite in contact with the skarn.

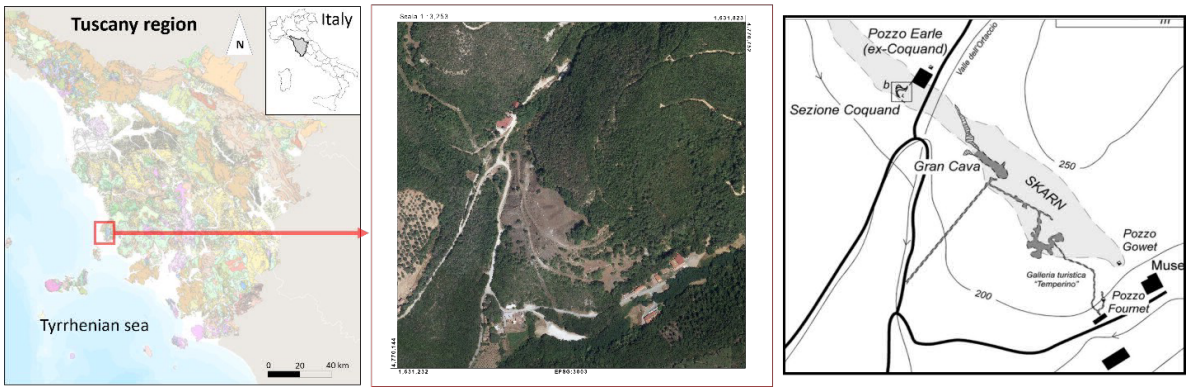

FIGURE 1: Case study location. Left: Temperino mine area in Tuscany region. Center: zoom on the Temperino mine hill. Right: a sketch of the first level of the mine, modified from [11].

2. TRANSMISSION-BASED MUOGRAPHY

The transmission-based muography (TM) technique used to obtain transmission and density maps relies on an accurate track reconstruction of hitting muons arriving within the MIMA muon detector acceptance cone (approximately $\pm 60^\circ$ with respect to the zenith; Figure 2).

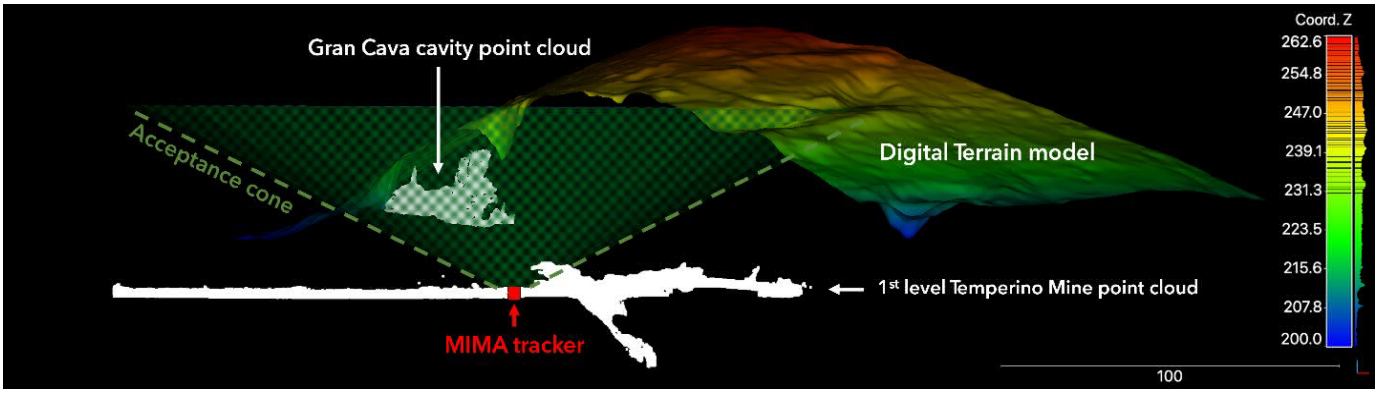

FIGURE 2: A cross section of the Temperino mine hill, modified from [4]. The red square indicates the measurement point. The green cone indicates the acceptance cone of the used tracker (approximately $\pm 60^\circ$), and the color scale on the left represents the height, in meters above sea level, of the digital terrain model.

The TM relies on two configuration measurements [4, 5]: target and free-sky. The former refers to the muon flux measurement conducted inside the mine gallery, where the rock mass between the detector and the surface is defined as the target, whereas the latter refers to the muon flux measurement conducted outside the mine, only pointing to the sky (free-sky), while maintaining the same orientation as the underground target measurement.

We define the measured muon transmission as T_m:

$$T_m = \frac{\phi_{m,\text{target}}(\theta, \varphi)}{\phi_{m,\text{free-sky}}(\theta, \varphi)}, \tag{1}$$

where $\phi_{m,\text{target}}$ is the muon flux measured underground, $\phi_{m,\text{free-sky}}$ is the muon flux measured at the surface in the free-sky configuration, and (θ, φ) are the zenith and azimuth angles, respectively: θ is the angle between the vertical direction and the line of sights (LoS), and φ is the clockwise angle from North direction.

The measured flux is defined as follows:

$$\phi_m(\theta, \varphi) = \frac{N(\theta, \varphi)}{t A_{\text{eff}}(\theta, \varphi)}, \tag{2}$$

where $N(\theta, \varphi)$ is the number of reconstructed muon tracks coming from various directions, t is the acquisition time, and $A_{\text{eff}}(\theta, \varphi)$ is the effective area of the tracker and depends on the acceptance of the detector and the trigger efficiency.

For the target and free-sky configuration measurements, the acceptance surface remains the same and variations in trigger efficiency are negligible. For this reason, $A_{\text{eff}}(\theta, \varphi)$ remain constant and T_m can be simplified as follows:

$$T_m(\theta, \varphi) = \frac{N_{\text{target}}(\theta, \varphi)}{N_{\text{free-sky}}(\theta, \varphi)} \cdot \frac{t_{\text{free-sky}}}{t_{\text{target}}}. \tag{3}$$

The $T_m(\theta, \varphi)$ values can then be compared to those obtained from the simulations carried out using some custom algorithms. The simulations were performed using the available three-dimensional data obtained from the digital terrain model (DTM) of the area and a terrestrial laser scanner (TLS) survey of underground accessible spaces (Figure 2). These three-dimensional data allowed us to obtain the rock thickness along each LoS of the tracker.

The opacity X is defined as follows, assuming that there are no voids or anomalies in the traversed rock:

$$X(\theta, \varphi, \bar{\rho}) = \int_{\text{LoS}} \rho \, dL = \bar{\rho}(\theta, \varphi) \cdot L(\theta, \varphi), \tag{4}$$

where ρ is the traversed matter density, $\bar{\rho}(\theta, \varphi)$ is the average density along the LoS, and $L(\theta, \varphi)$ is the distance between the terrain surface and the center of the tracker.

In this study, a single TM measurement location dataset was analyzed. The simulated transmission $T_s(\theta, \varphi, \bar{\rho})$ is defined in the same way as $T_m(\theta, \varphi)$ but with simulated muon fluxes:

$$T_s(\theta, \varphi, \bar{\rho}) = \frac{\phi_{S,\text{target}}(\theta, \varphi, \bar{\rho})}{\phi_{S,\text{free-sky}}(\theta, \varphi)}. \tag{5}$$

The latter are defined as follows:

$$\phi_{s,\text{target}}(\theta, \varphi, \bar{\rho}) = \int_{E_{\min}(X)}^{\infty} j(\theta, \varphi, E) dE, \tag{6}$$

$$\phi_{s,\text{free-sky}}(\theta, \varphi) = \int_{E_0}^{\infty} j(\theta, \varphi, E) dE, \tag{7}$$

where $j(\theta, \varphi, E)$ is the differential muon flux as a function of muon trajectories (θ, φ) and muon energy (E). The lower integral limit $E_{\min}(X)$ is the minimum energy that a muon must have to be detected by the MIMA tracker in the target configuration and is calculated by using tabulated values present in the literature [14]. The lower integral limit E_0 provides the same information as $E_{\min}(X)$ but for the free-sky configuration considering the opacity of the detector itself. For the differential muon flux, the values measured by the ADAMO experiment were used [1, 7, 15]. Therefore, the TM technique quantifies the reduction of the muon flux intensity owing to the thickness and density of the studied target and, through the comparison with the $T_s(\theta, \varphi, \rho)$, making it possible to associate density values to each LoS.

The TM technique is usually exploited to study relatively large objects such as mines, volcanoes, and mountains [16, 17, 18, 19] and provides two-dimensional transmission and density maps of the studied target within the LoS of the tracker. The analysis of these output maps enables the identification of density anomalies that may be associated with unknown cavities or dense objects (ore shoots) between the tracker and the terrain surface [5]. Furthermore, starting from the two-dimensional data of the final maps, it is possible to reconstruct in a three-dimensional way the objects of interest, namely, anomalies corresponding to denser areas (ore shoots) or less dense ones (cavities). To delve into this process, please refer to the works listed in the bibliography [5, 20].

3. RESULTS

For this work, the data acquired by the MIMA tracker at the measurement point shown in Figure 2 were analyzed. The detector was located inside the first level of the Temperino mine, about 50 m below the terrain surface, and acquired more than 1×10^6 events in 67 days. The choice of this measurement point was not random but has been defined based on three criteria: proximity to the tourist path, the presence of one known cavity above the detector (Gran Cava; Figure 2), and the potential presence of Fe-Cu enriched veins. The first reason was related to the MIMA-SITES project, through which these measurements were conducted, aiming to verify this imaging technique for safety, archaeology, and mining assessments aligned with the park's interests. The second reason was the presence of a known cavity that allowed for a real comparison of muography's cavity identification and reconstruction capabilities. The third reason pertains to the hypothesis of the presence of Cu-Fe enriched veins never exploited during mining activities. Furthermore, accessibility was also considered for the electrical supply, but not as the main criterion, since we wanted to test the detector and our technology, even in less favorable environments, such as narrow and humid spaces. Regarding constraints linked more closely to muon physics, we primarily considered the potential acquisition times relative to depth to ensure obtaining a valid statistical sample within a reasonable timeframe for the duration of the MIMA-SITES project.

The TM-obtained maps are shown in Figure 3. In Figure 4, it is possible to visualize a two-dimensional cross section extrapolated from the three-dimensional environment.

The polar maps show the calculated relative transmission and average density values along each LoS of the MIMA tracker. Both maps clearly show areas of lower density corresponding to known (the Gran Cava cavity) and unknown cavities. The latter are believed to correspond to ancient voids created during mining cultivation, inaccessible for a long time, and absent in the mapping of tunnels related to mining activities in the last century. The isolation of these unknown cavities is mainly due to the collapses of unstable ceilings. Moreover, an oriented ore shoot is visible. The latter was called "snake-shaped" body and was confirmed by several underground and surficial field surveys. This high-density body is characterized by a well-defined NNW-SSE orientation and a subvertical geometry, which is consistent with the general setting of the emplaced skarn and mafic porphyry exploited in the past in this mine [11, 21]. By correlating geological knowledge with the TM results, it was possible to observe that the "snake-shaped" body has a 2–4 m thickness, with average density values along the LoS, ranging from 3.0 to 3.4 g/cm^3. This high-density body is in contact with lower-density host rocks of approximately 2.5–2.9 g/cm^3. All these data allowed us to interpret the "snake-shaped" body as a mafic porphyry intrusion associated with the relative metamorphic contact rocks generated through interactions with the host skarn body. The Cu-Fe ores overprinted the skarn rocks at contact with the mafic porphyry intrusions and dikes, with mineral assemblages dominated by chalcopyrite, pyrite, and pyrrhotite (density up to 4-5 g/cm^3). Obviously, the TM technique returns average density values along the various LoS of the detector; therefore, these density values often underestimate the higher density value present along each LoS.

4. CONCLUSIONS

This study shows a real application of TM to image the inner portion of a skarn body outcropping at the Temperino mine in the San Silvestro Archaeological and Mining Park (Italy). This work shows one of the first applications of muon radiography for skarn ore shoot prospecting in the field of mining exploration. To accomplish this objective, it was necessary to combine the TM output with an in-depth geological understanding of the study area. The obtained results highlight the potential of muon radiography for mining activities.

This study allowed us to verify the reliability of TM for the visualization of the inner structures belonging to the rock bodies overlying the muon detector and to validate muography as a support tool for other classical mining exploration methods to visualize underground rock density difference distributions, to indicate the presence of potential ore bodies (or cavities), and to provide indications for the directions of future excavations or drilling. Furthermore, we confirm that even a single TM measurement can provide useful information about ore deposits.

In this proceeding, we deliberately present only 2D results to simplify understanding, making the potential of the technique clear to future readers even with just the 2D results (Figures 3 and 4). As explained in [4] (and [19]), it is possible to achieve a 3D reconstruction in addition to the typical 2D output for both ore-body and cavities, relatively. The interested reader can freely delve deeper into the articles listed in the bibliography, which explain the 3D reconstruction technique. Nevertheless, there are some issues to be resolved:

(i) to find a way to make tracker installation more rapid and easier,

(ii) to plan topographical and field surveys correctly to achieve reliable simulations,

(iii) to correctly assess errors in the muon imaging process and results, particularly those related to potential bias introduced by misalignments, during the comparison with the free-sky configuration.

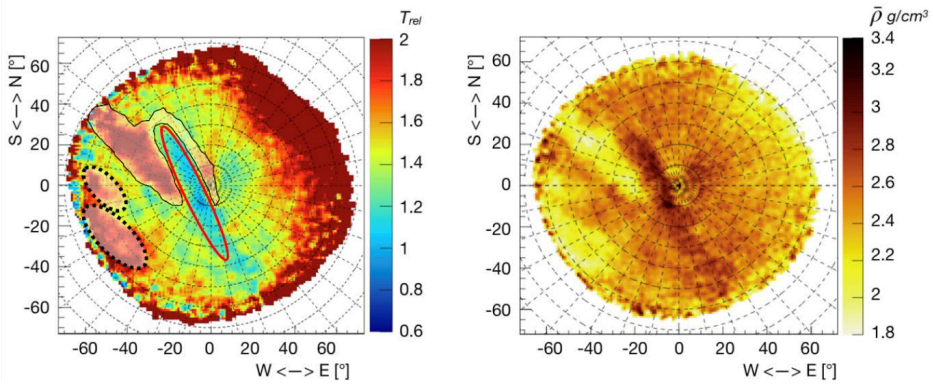

FIGURE 3: Left: polar map of the relative transmission for $\bar{\rho}(\theta, \varphi) = 3.2\,g/cm^3$, the red ellipse highlights the high-density ore shoot, the dotted black lines identify two unknown cavities, and the continuous black line shows the perimeter of the Gran Cava cavity. Right: polar map of the average densities. Modified from [4].

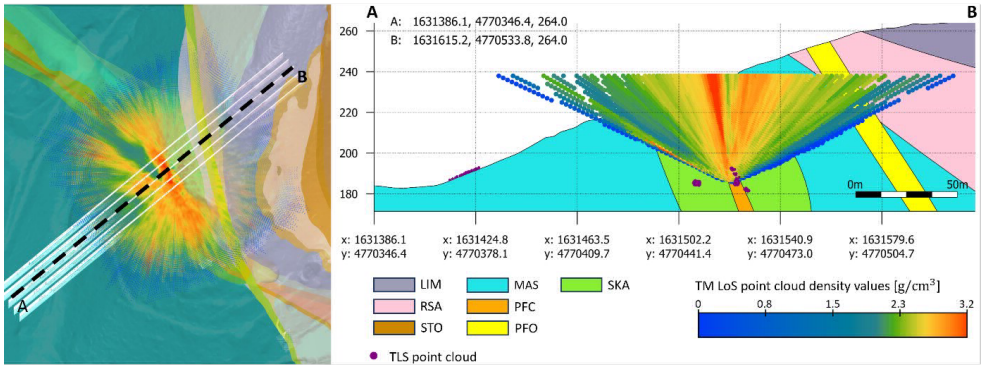

FIGURE 4: Right: orthogonal view of the geological map at the Temperino mine with the directional density values obtained from the muography survey. AB identifies the section shown on the right. Right: AB cross section showing the results of TM-obtained density values along the various LoS of the MIMA tracker. LIM: Calcare Selcifero di Limano Formation; RSA: Rosso Ammonitico Formation; STO: Tuscan succession; MAS: Calcare Massiccio; PFC: Coquand Felsic dike; PFO: Ortaccio Felsic dike; SKA: Skarn.

The workflow described in this paper is suitable for scenarios in which a mine gallery already exists. Further measurements will be conducted in the Temperino mine gallery to better understand the shape and extension of the identified ore shoot.

The major future objectives of our research group concern the speeding of muographic data analysis and processing, as well as the comprehension of the impact of field surveys and topographical data on the reliability of the muon imaging results.

CONFLICTS OF INTEREST

The authors declare that there are no conflicts of interest regarding the publication of this paper.

ACKNOWLEDGMENTS

The presented results were achieved thanks to the collaboration between the National Institute for Nuclear Physics (INFN), Division of Florence, the Department of Earth Science of the University of Florence, and the Parchi Val di Cornia S.p.A within the MIMA-SITES project. We thank the underground support of the Institute of Geosciences and Georesources CNR of Pisa.

References

[1] Baccani G., Bonechi L., Bongi M., Brocchini D., Casagli N., Ciaranfi R., et al. Muon Radiography of Ancient Mines: The San Silvestro Archaeo-Mining Park (Campiglia Marittima, Tuscany). Universe 2019;5:34. https://doi.org/10.3390/universe5010034.

[2] Zhang Z.-X., Enqvist T., Holma M., Kuusiniemi P. Muography and Its Potential Applications to Mining and Rock Engineering. Rock Mech Rock Eng 2020;53:4893-907. https://doi.org/10.1007/s00603-020-02199-9.

[3] Holma M., Zhang Z., Kuusiniemi P., Loo K., Enqvist T. Future Prospects of Muography for Geological Research and Geotechnical and Mining Engineering. In: Oláh L., Tanaka H. K. M., Varga D., editors. Geophys. Monogr. Ser. 1st ed., Wiley; 2022, p. 199–219. https://doi.org/10.1002/9781119722748.ch15.

[4] Beni T., Borselli D., Bonechi L., Bongi M., Brocchini D., Ciaranfi R., et al. Transmission-Based Muography for Ore Bodies Prospecting: A Case Study from a Skarn Complex in Italy. Nat Resour Res 2023. https://doi.org/10.1007/s11053-023-10201-8.

[5] Borselli D., Beni T., Bonechi L., Bongi M., Brocchini D., Casagli N., et al. Three-dimensional muon imaging of cavities inside the Temperino mine (Italy). Sci Rep 2022;12:22329. https://doi.org/10.1038/s41598-022-26393-7.

[6] Baccani G. Construction and calibration of the MIMA cosmic ray tracker for applications related to muon radiography and first measurements, Master's degree thesis in Physical Sciences and Astrophysics, UNIFI, AA 2016/2017. 2016.

[7] Borselli D. Muographic study of the Temperino mine with the MIMA detector: development and test of an algorithm for identification and reconstruction of cavities in three dimensions. Master's degree thesis in Physical and Astrophysical Sciences. University of Florence, Faculty of Mathematical, Physical and Natural Sciences, 2018.

[8] Baccani G., Bonechi L., Borselli D., Ciaranfi R., Cimmino L., Ciulli V., et al. The MIMA project. Design, construction and performances of a compact hodoscope for muon radiography applications in the context of archaeology and geophysical prospections. J Instrum 2018;13:P11001-P11001. https://doi.org/10.1088/1748-0221/13/11/P11001.

[9] Bonechi L., Ambrosino F., Cimmino L., D'Alessandro R., Macedonio G., Melon B., et al. The MURAVES project and other parallel activities on muon absorption radiography. EPJ Web Conf 2018;182:02015. https://doi.org/10.1051/epjconf/201818202015.

[10] Cimmino L., Ambrosino F., Bonechi L., Ciaranfi R., D'Alessandro R., Masone V., et al. The MURAVES telescope front-end electronics and data acquisition. Ann Geophys 2017;60:4. https://doi.org/10.4401/ag-7379.

[11] Da Mommio A., Iaccarino S., Vezzoni S., Dini A., Rocchi S., Brocchini D., et al. Valorizzazione del geosito "Sezione Coquand", miniera del Temperino (Parco Archeominerario di San Silvestro, Campiglia Marittima). Atti Della Soc Toscana Sci Nat Resid Pisa Mem Ser A 2010:55–72. https://doi.org/10.2424/ASTSN.M.2010.07.

[12] Vezzoni S., Dini A., Rocchi S. Reverse telescoping in a distal skarn system (Campiglia Marittima, Italy). Ore Geol Rev 2016;77:176–93. https://doi.org/10.1016/j.oregeorev.2016.03.001.
[13] Beni T., Baccani G., Borselli D., Bonechi L., Bongi M., Brocchini D., et al. Absorption-based muography for ore bodies prospecting: a case study from Temperino Mine (Italy). display; 2022. https://doi.org/10.5194/egusphere-egu22-8837.
[14] Groom D. E., Mokhov N. V., Striganov S. I. Muon Stopping Power and Range Tables 10 MeV–100 TeV. At Data Nucl Data Tables 2001;78:183–356. https://doi.org/10.1006/adnd.2001.0861.
[15] Bonechi L., Bongi M., Fedele D., Grandi M., Ricciarini S. B., Vannuccini E. Development of the ADAMO detector: test with cosmic rays at different zenith angles. 29th Int. Cosm. Ray Conf. Pune, vol. 9, 2005, p. 283–6.
[16] Bonechi L., D'Alessandro R., Giammanco A. Atmospheric muons as an imaging tool. Rev Phys 2020;5:100038. https://doi.org/10.1016/j.revip.2020.100038.
[17] D'Alessandro R., Ambrosino F., Baccani G., Bonechi L., Bongi M., Caputo A., et al. Volcanoes in Italy and the role of muon radiography. Philos Trans R Soc Math Phys Eng Sci 2019;377:20180050. https://doi.org/10.1098/rsta.2018.0050.
[18] Tanaka H. K. M., Nakano T., Takahashi S., Yoshida J., Ohshima H., Maekawa T., et al. Imaging the conduit size of the dome with cosmic-ray muons: The structure beneath Showa-Shinzan Lava Dome, Japan. Geophys Res Lett 2007;34:L22311. https://doi.org/10.1029/2007GL031389.
[19] Tanaka H. K. M., Kusagaya T., Shinohara H. Radiographic visualization of magma dynamics in an erupting volcano. Nat Commun 2014;5:3381. https://doi.org/10.1038/ncomms4381.
[20] Bonechi L., D'Alessandro R., Mori N., Viliani L. A projective reconstruction method of underground or hidden structures using atmospheric muon absorption data. J Instrum 2015;10:P02003-P02003. https://doi.org/10.1088/1748-0221/10/02/P02003.
[21] Vezzoni S. Evolution of a pluton-porphyry-skarn system: the Temperino-Lanzi mine (Campiglia Marittima, Tuscany). PhD Thesis. Università di Pisa, 2014.